tion of a greater loading rate of 33 mm/year for the Parkfield $M = 6$ sequence (*21*). The resulting relation is $v = 10^{(0.105M_w+0.45)}/T_{av}$, where v is in cm/year, T_{av} is the average recurrence interval for the sequence in years, and M_w is the moment magnitude. At a lower magnitude threshold of $M_w = 1.15$, we would not expect repeaters if slip rates were less than 3 mm/year for the 16-year period.

23. A. L. Thomas, thesis, Stanford University, Stanford, CA (1993).
24. R. Bürgmann, E. Fielding, J. Sukhatme, *Geology* **26**, 559 (1998).
25. R. Simpson (unpublished data) independently developed similar three-dimensional models of a frictionless Hayward fault, concluding that surface creep rates do not require a locked northern fault segment.
26. D. F. Argus and R. G. Gordon, *Geology* **19**, 1085 (1991).
27. F. Waldhauser, W. L. Ellsworth, A. Cole, *Geophys. Res. Lett.* **26**, 3525 (1999).
28. Supported by grants from the NSF Geophysics program, NASA's Solid Earth and Natural Hazards program, and the U.S. Geological Survey (USGS) National Earthquake Hazards Reduction Program. Seismic and geodetic data are archived at the Northern California Earthquake Data Center (NCEDC). F. Waldhauser kindly shared his relocated earthquake catalog shown in Fig. 2A and W. Prescott generously provided USGS GPS data. Berkeley Seismological Laboratory contribution 00-06.

28 April 2000; accepted 22 June 2000

Remobilization in the Cratonic Lithosphere Recorded in Polycrystalline Diamond

D. E. Jacob,[1]* K. S. Viljoen,[2] N. Grassineau,[3] E. Jagoutz[4]

Polycrystalline diamonds (framesites) from the Venetia kimberlite in South Africa contain silicate minerals whose isotopic and trace element characteristics document remobilization of older carbon and silicate components to form the framesites shortly before kimberlite eruption. Chemical variations within the garnets correlate with carbon isotopes in the diamonds, indicating contemporaneous formation. Trace element, radiogenic, and stable isotope variations can be explained by the interaction of eclogites with a carbonatitic melt, derived by remobilization of material that had been stored for a considerable time in the lithosphere. These results indicate more recent formation of diamonds from older materials within the cratonic lithosphere.

Cratons—the nuclei of continents—preserve relicts of Earth's oldest geologic record. The occurrence of diamonds in samples from Earth's mantle is restricted to cratonic areas (*1*), and radiogenic isotope studies of their inclusions revealed similarly old ages [3.4 to 3.6 billion years ago (Ga)] for diamond genesis in the cratonic lithosphere (*2*, *3*). Recently, however, geochemical evidence indicates the formation of diamond earlier than 1 Ga (*4*), and seismic tomography has indicated that cratonic roots have variable depths (*5*), suggesting that cratonic lithosphere is more dynamic.

Aggregates of polycrystalline diamond (framesites) (*6*) from kimberlites often contain interstitial silicates and/or sulfides of lherzolitic or eclogitic paragenesis. Both these parageneses are known from xenoliths in kimberlites and inclusions in diamonds (*7*). The small grain size of the diamonds is consistent with rapid crystallization, and the intimate intergrowth of silicates and diamond indicates contemporaneous crystallization. Framesites occur in several kimberlite pipes in southern Africa (e.g., Venetia, Premier, Jwaneng, and Orapa) and can make up several percent of the total diamond concentration in a mine.

We focused on framesites containing silicates of eclogitic affinity from the Venetia kimberlite pipe situated in the Limpopo central belt in northeastern South Africa (*8*). All samples chosen for this study contain 10 to 25 weight % (wt %) (≈0.9 to 1.4 g) eclogitic garnet, but none contain clinopyroxene. One sample (V948) contains about 1% sulfide. Eclogitic garnets from framesites have more restricted Ca contents that are generally lower than those of garnets from eclogitic xenoliths and eclogitic inclusions in diamond (*9*). However, elevated Cr_2O_3 contents, which would be expected for websteritic garnets, are not present. Mg numbers (*10*) of eclogitic garnets in framesites (Table 1) are mostly higher at lower TiO_2 concentrations than those of diamond inclusions and eclogite xenoliths. Additionally, a trend of increasing Mg number with increasing TiO_2 content is apparent, which is not reported for eclogite xenoliths and inclusions in diamond, nor is it readily explained by common rock-forming processes such as fractional crystallization. We chose samples representative of this trend and large enough to be able to carry out a complete study of major and trace elements, Rb-Sr, Nd-Sm isotopes, and oxygen isotopes on mineral separates, as well as of carbon isotopes on the diamonds.

On an isochron plot of $^{147}Sm/^{144}Nd$ versus $^{143}Nd/^{144}Nd$, the garnets fall on a straight line that, if interpreted as an isochron, yields an apparent age of 125 million years ago (Ma). The Venetia kimberlite itself, however, is 533 Ma (*8*), indicating that this line results from a mixing relation. In fact, the initial Nd isotopic ratios (measured $^{143}Nd/^{144}Nd$ ratios recalculated to the age of the kimberlite) also correlate with most other chemical parameters of the framesites, such as Mg numbers, $\delta^{18}O$ values, and ratios of trace elements in the garnets, further supporting mixing. Furthermore, stable isotope measurements display correlations between chemical parameters of the garnets (e.g., Mg number and $\delta^{18}O$) and the carbon isotopic composition of the diamond crystals (Fig. 1). Systematic relations between host diamonds and their inclusions are virtually unknown for macrocrystalline diamonds (*11*) but are reported for framesites from Orapa (Botswana) (*12*) (Fig. 1), implying that mixing could be a general process in framesite genesis worldwide.

In contrast to garnets from most eclogite xenoliths, all framesite garnets have $\varepsilon_{Nd(i)}$ values between −15.9 and −21.7 (Fig. 2). The correlation between $^{87}Sr/^{86}Sr$ and $^{143}Nd/^{144}Nd$ ratios, the mixing line, points to an end-member with even more unradiogenic Sr and Nd isotopic values. The unradiogenic Nd isotopes require an old, long-term light rare earth element (LREE)–enriched component, reminiscent of that identified in harzburgitic subcalcic garnets included in diamond (*13*). However, Sm/Nd ratios of the framesitic garnets are too high to account for the unradiogenic $^{143}Nd/^{144}Nd$ ratios and show that the isotopic signature must be inherited.

All four garnets show similar trace element patterns with high heavy rare earth element (HREE) and low LREE contents that are typical for garnets (Fig. 3A). However, trace element zonation detected by in situ trace element measurements in one of the samples (V948) shows that framesite formation may have occurred shortly before kimberlite eruption. Figure 3B shows zones detected by time-resolved laser ablation inductively coupled plasma mass spectrometry (ICP-MS) (LAM) analysis in sample V948 that are enriched in many incompatible elements and LREE. In these zones, which cannot be attributed to cores or rims, Sr contents are enriched by up to a factor of 19 and are accompanied by an enrichment in LREE, similar to features of

[1]Institut für Geologische Wissenschaften, Universität Greifswald, F.-L. Jahnstrasse 17a, D-17487 Greifswald, Germany. [2]DeBeers Geoscience Center, Post Office Box 82232, Southdale 2135, South Africa. [3]Department of Geology, Royal Holloway University of London, Egham, Surrey TW20 0EX, UK. [4]Max-Planck Institut für Chemie, Saarstrasse 23, D-55122 Mainz, Germany.

*To whom correspondence should be addressed.

peridotitic diamond inclusions (*4*). The mineral separate of V948 used for radiogenic isotope measurements shows different enrichment that is stronger for Nd and Sm (factor of 8) than for Sr (factor of 5) compared with the zonation detected by LAM. However, major elements in these garnet grains are homogeneous.

We interpret these variable trace element contents in garnet grains from sample V948 as zonation due to growth in a fractionating melt. An origin by alteration on cracks or by minute inclusions of different phases such as carbonate or apatite can be excluded because neither was observed and they would be easily detected by time-resolved LAM analysis (*14*).

Rapid growth or metasomatism by kimberlite-related fluids or melts may cause zonations in minerals, but this can be excluded for Venetia, which is a Group I kimberlite (*8*) and has a much more radiogenic $^{87}Sr/^{86}Sr$ signature of 0.7048 (Fig. 2) as well as four orders of magnitude higher Sr contents. This would cause much higher $^{87}Sr/^{86}Sr$ values by metasomatic interaction with fluids than is observed.

Trace element zonations in minerals are transient features at temperatures typical for Earth's mantle and may not survive over billions of years. Shimizu and Sobolev (*4*) described similar, but for Sr more spectacular, trace element zonations in a peridotitic garnet included in a diamond and calculated a maximum homogenization time of 7×10^4 years at temperatures typical for diamond formation (1000°C) for a grain of 100-μm radius. The maximum homogenization time at 800°C is 3×10^6 years for a 100-μm grain (*15*). Diffusion coefficients for Sr in eclogitic garnets are not known but may be similar within an order of magnitude to the experimental values used for peridotitic garnet (*4*). Temperatures below 1000°C would be atypical for the diamond zone in the cratonic lithosphere, as this temperature corresponds to the intersection of a typical 40 mW/m^2 cratonic geotherm with the diamond-graphite phase boundary (*16*). There is no evidence from paleogeotherms derived from mantle xenoliths that colder conditions existed. The preservation of trace element zonation implies that the framesites are young and were entrapped in the kimberlite shortly after their formation. Chemical characteristics, however, suggest that they are genetically unrelated to the kimberlite.

The Venetia framesites are consistent with a model of a two-component mixing of end-members that were distinct in chemical composition, although both are required to contain carbon of distinct isotopic composition and probably different concentrations to account for the covariation in Fig. 1. End-member A is suggested to be a carbonatitic melt, characterized by chemical parameters extrapolated from the compositionally most extreme sample V911: high Mg number (>81) and TiO_2 contents, low $\delta^{18}O$ [<6.5 per mil (‰)] and $\delta^{13}C$ values (<−23‰), and unradiogenic Nd and Sr isotopic compositions. The radiogenic isotopes argue for an old, Rb-depleted end-member that was enriched in Nd relative to Sm. Although low Rb does not correspond to carbonatites found at Earth's surface, it has been found in mantle carbonates (*17*). The crystal sites of carbonate minerals can accommodate Nd better than Sm, but not Rb, translating into time-integrated negative ε_{Nd} values, but low Rb/Sr ratios leading to low $^{87}Sr/^{86}Sr$. The carbonate-bearing source area was isolated over sufficient time to develop an unradiogenic Nd isotopic signature, whereas the melt itself was generated shortly before framesite formation. The high Mg number of garnets may be consistent with carbonate-bearing assemblages at these high pressures (*18*).

$\delta^{13}C$ values as low as −24‰, the most extreme value observed in the framesite sample suite, could be generated by repeated carbonate precipitation from a CO_2-carbonate system within Earth's mantle (*19*) in which the carbon is primordial in origin (*20*). How-

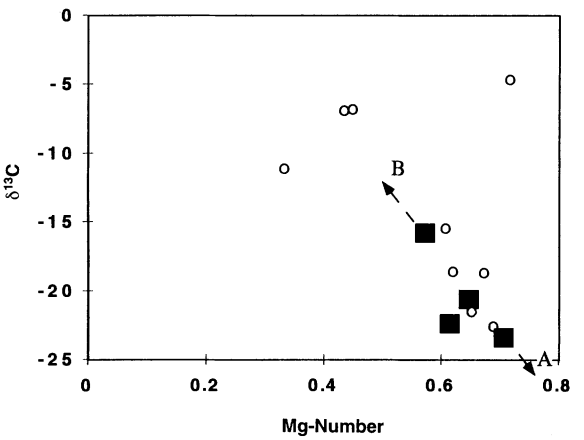

Fig. 1. Mg numbers of the Venetia garnets correlate with $\delta^{13}C$ values of the coexisting diamonds (■). Circles are data from the Orapa Mine, Botswana (*12*). Dashed arrows point to hypothetical end-members "A" and "B."

Table 1. Major elements (wt %), Nd, Sm, Sr, Rb (parts per million), radiogenic isotopes, $\delta^{18}O$, and $\delta^{13}C$ (‰) of framesitic garnets and associated diamonds. Major elements were measured by electron microprobe at the De Beers Geoscience Center by methods described in (*31*). Trace elements except Rb were measured by isotope dilution with blanks of 5 pg for Nd, 15 pg for Sm, and 25 pg for Sr. Rb* concentrations were measured by LAM with analytical errors of 7%. Values for V919 and V925 are maximum values. Sm-Nd and Rb-Sr chemistry and isotopic measurements were carried out as described in (*23*). Uncertainties are $\Sigma 2\sigma_n/\sqrt{n-1}$ analytical errors in the last decimal place. Oxygen isotopes were measured by laser fluorination (*32*); carbon isotopes were measured by standard methods (*33*) at Laboratoire de Géochimie des Isotopes Stables, Institut de Physique au Globe, Université Paris, and are averages of two analyses. Uncertainties are based on reproducibility and reported for the last decimal place. $\delta^{18}O$ and $\delta^{13}C$ are the difference in $^{18}O/^{16}O$ and $^{13}C/^{12}C$ in ‰ relative to SMOW (standard mean ocean water) and PDB (Pee Dee belemnite).

	V911	V919	V925	V948
SiO_2	41.98	41.93	41.28	40.80
TiO_2	0.49	0.40	0.31	0.23
Al_2O_3	22.62	22.31	22.77	22.96
Cr_2O_3	0.14	0.34	0.12	0.12
FeO	8.75	10.76	11.45	13.06
MnO	0.26	0.29	0.30	0.31
MgO	20.85	19.04	18.17	17.38
CaO	4.45	4.44	4.84	4.93
Na_2O	0.07	0.07	0.04	0.05
K_2O	0	0.01	0	0
Total	99.61	99.59	99.28	99.84
Mg number	80.9	75.9	73.9	70.3
Nd	0.4561 ± 5	0.5165 ± 8	0.856 ± 2	7.16 ± 1
Sm	0.523 ± 1	0.534 ± 1	0.827 ± 4	7.394 ± 9
Sr	0.2416 ± 5	0.296 ± 1	0.963 ± 4	2.988 ± 3
Rb*	0.016	0.02	0.02	0.19
$^{143}Nd/^{144}Nd$	0.513271 ± 14	0.513209 ± 17	0.513178 ± 19	0.513219 ± 16
$^{147}Sm/^{144}Nd$	0.6987	0.6314	0.5864	0.6249
$^{87}Sr/^{86}Sr$	0.703193 ± 91	0.703589 ± 71	0.703189 ± 24	0.703379 ± 78
$^{87}Rb/^{86}Sr$	0.1657	0.1743	0.0556	0.1674
$\delta^{18}O$	6.49 ± 4	7.30 ± 2	7.81 ± 3	8.09 ± 5
$\delta^{13}C$	−23.4 ± 4	−21.1 ± 2	−22.3 ± 1	−15.8 ± 2

ever, a subducted source of carbon, e.g., from hydrothermally altered oceanic crust (*21*), appears equally possible.

End-member B has a lower Mg number (<70) and TiO_2 contents, $\delta^{18}O > 8‰$, $\delta^{13}C > -16‰$, and more radiogenic $^{143}Nd/^{144}Nd$ and $^{87}Sr/^{86}Sr$ and may be a carbon-bearing eclogite originating from seawater-altered subducted oceanic crust (*22*, *23*). A $\delta^{18}O$ value ≥8‰ falls into the range observed for eclogite xenoliths thought to be derived from seawater-altered subducted oceanic crust of 2 to 9‰ (*22*), and carbon in the form of carbonate, diamond, and/or graphite is stable in eclogite xenoliths from the mantle.

The eclogitic framesites formed from a carbonatitic melt in the mantle containing isotopically light carbon and unradiogenic Nd isotopic values that remobilized components of carbon-bearing eclogite. Trace element zonation shows that crystallization was rapid, and its preservation implies that crystallization occurred shortly before kimberlite eruption. It appears that framesites are formed by processes not detected in the majority of macrocrystalline diamonds (although intergrowths of these with polycrystalline diamond can be found) and therefore represent a distinct diamond reservoir. They indicate that young remobilization processes do indeed occur within the cratonic roots.

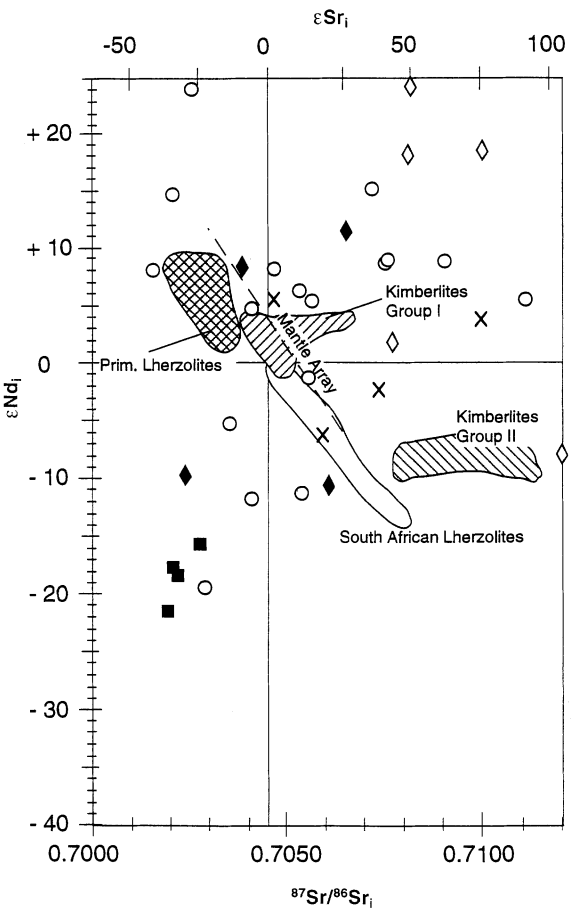

Fig. 2. Initial ε_{Nd} values and $^{87}Sr/^{86}Sr$ ratios for garnets from eclogite xenoliths from Siberia (*23*, *34*) (○, nondiamondiferous; ◇, diamondiferous) and southern Africa (*30*, *31*, *35*) (×, nondiamondiferous; ◆, diamondiferous) compared with framesite garnets (■, this study). All isotopic ratios are recalculated to the age of the respective kimberlite. Venetia is a Group I kimberlite. $\varepsilon_{Nd(i)} = \{[(^{143}Nd/^{144}Nd)_m/(^{143}Nd/^{144}Nd)_t^{CHUR}] - 1\} \times 10{,}000$, where "m" is the measured value and "t" is that for CHUR (Chondrite Uniform Reservoir) at 533 Ma.

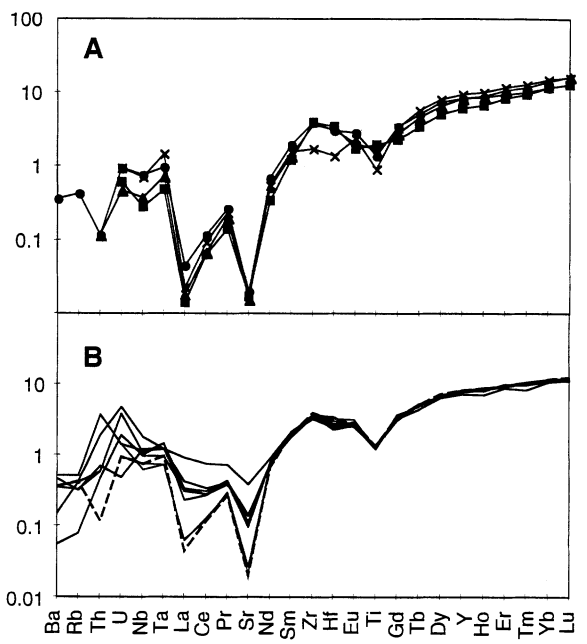

Fig. 3. (**A**) Trace elements in four garnets normalized to primitive mantle (*36*). Measurements were made in situ by LAM at the Memorial University, St. John's (Newfoundland) (*37*). ▲, V919; ■, V911; ×, V925; ●, V948. (**B**) Zones variably enriched in trace elements from several grains in sample V948. The dashed line indicates the homogeneous sample from (A) for comparison. All other samples appeared to be homogeneous.

References and Notes

1. A. J. A. Janse, *Russ. Geol. Geophys.* **33**, 9 (1992).
2. S. H. Richardson *et al.*, *Nature* **310**, 198 (1984).
3. S. H. Richardson *et al.*, *Nature* **346**, 54 (1990).
4. N. Shimizu and N. V. Sobolev, *Nature* **375**, 394 (1995).
5. F. J. Simons *et al.*, *Lithos* **48**, 17 (1999).
6. J. J. Gurney and F. R. Boyd, *Yearb. Carnegie Inst.* **1982**, 267 (1982). Framesites are defined as polycrystalline aggregates of diamond with crystals smaller than 1 mm.
7. O. Navon, in *P. Nixon Volume*, J. Gurney *et al.*, Eds. (Red Roof Design, Cape Town, South Africa, 1999), pp. 584–604.
8. H. L. Allsopp *et al.*, *S. Afr. J. Geol.* **98**, 239 (1995).
9. CaO contents in eclogitic garnets from framesites range between 2.70 and 8.18 wt %, with an average of 4.73 wt % (*24*); those of garnets in eclogite xenoliths average 6.84 wt % (n = 182) and range between 3.3 and 21.69 wt % (*25*, *26*).
10. Mg number = $\frac{Mg}{Mg + Fe} \times 100$.
11. P. Deines *et al.*, *Geochim. Cosmochim. Acta* **61**, 3993 (1997). These authors report a negative correlation for $\delta^{13}C$ and wt % FeO in olivines from southern African peridotitic diamond inclusions.
12. T. E. McCandless *et al.*, paper presented at the 28th International Geological Congress, Washington, DC, 1989.
13. Subcalcic garnets are harzburgitic (depleted) minerals with low CaO contents (<2 wt %) but high Cr_2O_3 contents (up to 18 wt %) (*27*). Typically, they have LREE-enriched trace element signatures and unradiogenic $\varepsilon_{Nd(i)}$ values down to −60ε (*28*). Sm/Nd ratios are 0.02 to 0.80 (*29*).
14. All grains used for either isotope measurements or LAM were fresh and optically clear up to a magnification of 500 and were thoroughly acid leached after hand-picking (*30*) followed by optical rechecks. Inclusions of other minerals such as carbonate or apatite would also be evident from abrupt changes in the time-resolved signal for Ca and Si.
15. 1×10^{-18} cm/s^2: R. Coghlan, thesis, Brown University, Providence, RI (1990).
16. H. N. Pollack and D. S. Chapman, *Tectonophysics* **38**, 279 (1977).
17. D. Ionov *et al.*, *Earth Planet. Sci. Lett.* **119**, 283 (1993).
18. G. M. Yaxley and D. H. Green, *Earth Planet. Sci. Lett.* **128**, 313 (1994).
19. P. Cartigny, J. W. Harris, M. Javoy, *Science* **280**, 1421 (1998).
20. S. E. Haggerty, *Science* **285**, 851 (1999).
21. T. McCandless and J. J. Gurney, *Russ. Geol. Geophys.* **38**, 394 (1997).
22. D. Jacob and S. Foley, *Lithos* **48**, 317 (1999).

23. D. Jacob *et al.*, *Geochim. Cosmochim. Acta* **58**, 5191 (1994).
24. K. S. Viljoen, unpublished data.
25. C. J. Hatton, thesis, University of Cape Town, Cape Town, South Africa (1978).
26. I. D. MacGregor and W. I. Manton, *J. Geophys. Res.* **91**, 14063 (1986).
27. N. V. Sobolev, *Peep-Seated Inclusions in Kimberlites and the Problem of the Composition of the Upper Mantle* (at the American Geophysical Union, Washington, DC, 1977).
28. G. P. Pearson *et al.*, *Geochim. Cosmochim. Acta* **59**, 959 (1995).
29. D. Jacob *et al.*, *N. Jahrb. Miner. Abh.* **172**, 357 (1998).
30. D. Jacob and E. Jagoutz, in *Kimberlites, Related Rocks and Mantle Xenoliths*, CPRM Special Publication 1/95, H. O. A. Meyer and O. H. Leonardos, Eds. (Companhia de Pesquisa de Recursos Minerais, Brasilia, Brazil, 1995), vol. 1, pp. 304–317.
31. K. S. Viljoen *et al.*, *Chem. Geol.* **131**, 235 (1996).
32. D. Mattey and C. McPherson, *Chem. Geol.* **105**, 305 (1993).
33. P. Cartigny, thesis, Université Paris 7 (1997).
34. G. A. Snyder *et al.*, *J. Petrol.* **38**, 85 (1997).
35. C. B. Smith *et al.*, in *Kimberlites and Related Rocks*, J. Ross *et al.*, Eds., *Geol. Soc. Am. Spec. Publ.* **14**, 853 (1989).
36. S.-S. Sun and W. F. McDonough, in *Magmatism in the Ocean Basins*, A. D. Saunders and M. J. Norry, Eds., *Geol. Soc. London Spec. Publ.* **42**, 313 (1989).
37. H. P. Longerich *et al.*, *J. Anal. At. Spectrom.* **11**, 899 (1996). Trace element data are available at www.sciencemag.org/feature/data.1051804.shl.
38. This study was supported by Deutsche Forschungsgemeinschaft grants Ja 781/2-1 and Ja 781/2-2 to D.J. We thank D. Mattey for providing access to his efficient stable isotope lab and P. Cartigny for measuring the carbon isotopes. Framesite samples were provided by DeBeers. We thank three anonymous reviewers for constructive criticism.

1 May 2000; accepted 20 June 2000

Degradation of Outer Membrane Protein A in *Escherichia coli* Killing by Neutrophil Elastase

Abderr azzaq Belaaouaj,[1]* Kwang Sik Kim,[4] Steven D. Shapiro[1,2,3]

In determining the mechanism of neutrophil elastase (NE)–mediated killing of *Escherichia coli*, we found that NE degraded outer membrane protein A (OmpA), localized on the surface of Gram-negative bacteria. NE killed wild-type, but not OmpA-deficient, *E. coli*. Also, whereas NE-deficient mice had impaired survival in response to *E. coli* sepsis, as compared to wild-type mice, the presence or absence of NE had no influence on survival in response to sepsis that had been induced with OmpA-deficient *E. coli*. These findings define a mechanism of nonoxidative bacterial killing by NE and point to OmpA as a bacterial target in host defense.

After bacterial infection, neutrophils engulf and kill bacteria by oxidative and nonoxidative pathways. Nonoxidative mechanisms are less well defined, but they predominantly relate to the ability of peptides to alter the bacterial membrane permeability (*1*). NE has long been regarded as an antibacterial protein, but its mechanism of bacterial killing remains unclear (*2*). NE is a potent serine proteinase whose catalytic activity relies on the His-Asp-Ser triad (*3*). Recently, we have demonstrated that NE is required for host defense against Gram-negative, but not Gram-positive, bacteria (*4*). These findings prompted us to delineate the mechanism by which NE kills *E. coli*, a common and virulent pathogen.

Using immuno–electron microscopy (immuno-EM), we confirmed that NE was localized within the phagolysosomes following ingestion of *E. coli* by neutrophils (Fig. 1A) (*5, 6*). To determine whether the antibacterial activity of NE was related to its catalytic activity, we cultured *E. coli* [10^6 colony-forming units (CFUs)] with or without human NE (2 μM), and bacterial viability was monitored over time by plating serial dilutions. The addition of NE markedly decreased *E. coli* growth (Fig. 1B). This decrease in bacterial growth was dependent on the time of

[1]Department of Pediatrics, [2]Department of Medicine, and [3]Department of Cell Biology and Physiology, Washington University School of Medicine, St. Louis, MO 63110, USA. [4]Division of Infectious Diseases, Children's Hospital, Los Angeles, CA 90027, USA.

*To whom correspondence should be addressed. Present address: Division of Pulmonary and Critical Care Medicine, Washington University School of Medicine, 660 South Euclid Avenue, Campus Box 8052, St. Louis, MO 63110, USA; E-mail: belaaouaja@msnotes.wustl.edu

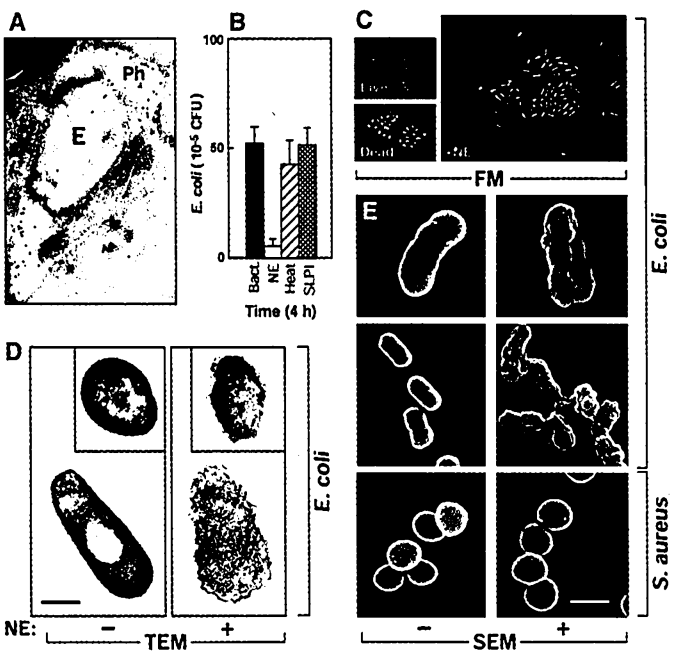

Fig. 1. NE localization and effect on bacteria. (**A**) Immuno-EM localization of NE in neutrophils. Human neutrophils were incubated with freshly grown bacteria at a 1:100 ratio, and the reactions were processed for immuno-EM with antibody to NE. A phagolysosome containing an *E. coli* bacterium is shown. There is an increased number of gold particles inside the phagolysosome. The estimated size of (A) is 3.5 μm. Ph, phagolysosome; E, *E. coli*. (**B**) NE kills *E. coli* through its catalytic activity. *E. coli* were incubated with or without NE. Similar experiments were repeated where NE was inactivated and viable bacterial counts were determined. SLPI (at 0.05 μM) inhibited NE activity (>95%) but exhibited unsubstantial antibacterial activity against *E. coli*. Results represent the mean of four experiments; error bars indicate the standard error of the mean. (**C**) Fluorescence microscopy (FM) of bacteria. *E. coli* were incubated without (live) or with NE (+NE) as described above, and the reactions were stained with a mixture of DAPI and SYTOX. DNA of live (intact cell membranes) and dead (disrupted membranes) bacteria fluoresce blue with DAPI and bright green with SYTOX (magnification, ×2000). (**D** and **E**) Electron micrographs of bacteria incubated with (+) or without (−) NE. *E. coli* and *S. aureus* were cultured with or without NE, and the reactions were processed for SEM and TEM. Single cells and aggregates of bacteria are shown. (**E**) In the presence of NE, the coccus morphology (*S. aureus*) remained intact, and the bacillus morphology (*E. coli*) was distorted (determined by SEM) (scale bar, 1.5 μm). (**D**) In the absence of NE, the outer and inner membranes are intact, but the addition of NE resulted in a distorted structure (determined by TEM) (scale bar, 0.5 μm). Insets represent cross sections of bacteria.